



# Growth and characterization of a nonlinear optical material: L-alanine DL-mandelic acid hemihydrate

P. Jayaprakash<sup>1</sup> · P. Rekha<sup>3</sup> · S. Sudha<sup>1</sup> · G. Vinitha<sup>4</sup> · M. Lydia Caroline<sup>1,2</sup>

Received: 9 March 2018 / Accepted: 11 July 2018 / Published online: 14 July 2018  
© Springer Science+Business Media, LLC, part of Springer Nature 2018

## Abstract

L-Alanine DL-mandelic acid hemihydrate (LADLMAH) an organic nonlinear optical chromophore crystal was synthesized using water as solvent and the crystals were grown by a slow solvent evaporation method. The single crystal X-ray diffraction study reveals that the crystals possess to triclinic system with acentric space group P1. The coordination of different moieties present in the compound and molecular structure were elucidated by vibrational and NMR spectroscopic studies. The lower cut-off wavelength is observed down to 258 nm and direct optical band gap was calculated as 5.20 eV. Second harmonic generation was confirmed by Kurtz–Perry powder method. Discrete thermodynamic properties were carried out by TG–DTA techniques. A multiple shot laser technique was adopted to investigate the surface laser damage of the crystal. The microhardness test was carried out employing one of the as-grown hard crystals and there by hardness number ( $H_V$ ) and Meyer's index ( $n$ ) were assessed. The dielectric behaviour of the grown crystal was studied for different temperatures at different frequencies. The third-order optical nonlinearity parameters of LADLMAH were investigated in detail using a Z-scan technique with Nd:YAG laser at 532 nm.

## 1 Introduction

At present electronic and photonic industry requires effective nonlinear optical materials such as laser crystals for wavelength conversion, optical amplification as well as the refractive index changes due to the intensity of laser source have gained considerable interest. Organic materials are expected to have relatively strong nonlinear optical properties due to delocalized electrons at  $\pi$ – $\pi^*$  orbital's configuration [1]. Nonlinear optical process provides the basis for key performance in optical switching and frequency conversion [2], which can be involved for a variety of applications varying from modulation of optical signals facilitated by the electro-optic effect [3]. Amino acids are interesting organic

materials for nonlinear optical applications as they contain a donor carboxylic (COOH) group and a proton acceptor amino ( $\text{NH}_2$ ) group known as zwitterions which create hydrogen bond networks [4] is requisite for the design of NLO chromophores. L-Alanine is non polar amino acid having equal number of amino and carboxyl groups and hence neutral. A wide range of second order NLO active materials composed of L-alanine have been synthesized, such as phosphoric acid admixed L-alanine [5], L-alanine hydrogen chloride monohydrate [6]. The present work deals synthesis of L-alanine an  $\alpha$ -amino acid mixed with DL-mandelic acid in the stoichiometric molar (1:1) ratio. The three dimensional crystal structure of the title compound elucidated by Hu et al. stated that the structure exhibit an optical separation of racemic mandelic acid in 1:1 stoichiometry of L-alanine and DL-mandelic acid [7]. Obviously the structure shows strong hydrogen bonding effects towards the neighbouring covalent bond such as between carbonyl and carboxylate groups and intermolecular hydrogen bonds between hydroxyl and carbonyl groups is the characteristic of amino acids. Also as detailed by Hu et al. [7], a short separation that exist between  $\text{O}\cdots\text{H}$ ,  $\text{C}\cdots\text{O}$  lead to intermolecular charge transfer and extreme hydrogen bond network between O and N contribute to molecular polarizability and dipole moment is the significance of amino acids in turn would find L-alanine

✉ M. Lydia Caroline  
lydiacaroline2006@yahoo.co.in

<sup>1</sup> Department of Physics, Arignar Anna Govt. Arts College, Cheyyar, Tamilnadu 604 407, India

<sup>2</sup> Department of Physics, Dr. Ambedkar Govt. Arts College, Vyasarpadi, Chennai 600 039, India

<sup>3</sup> Department of Physics, Bharathi Womens College, Chennai 600 108, India

<sup>4</sup> Division of Physics, School of Advanced Science, VIT University, Chennai 600 127, India

DL-mandelic acid hemihydrate (LADLMAH) as suitable and efficient candidate in the field of NLO applications. Some works based on mandelic acid have also been discussed in the literature [8–12]. LADLMAH, an organic NLO material was harvested by slow solvent evaporation technique using deionized water as solvent. In our paper we report the outcome of the various analyses such as spectral, optical, SHG, thermal, laser damage threshold, microhardness and dielectric and Z-scan studies performed on LADLMAH to prove it as an ideal candidate in nonlinear optical applications.

## 2 Materials and methods

### 2.1 Synthesis and crystal growth of LADLMAH

The LADLMAH single crystal was synthesized and grown by slow solvent evaporation technique. Stoichiometric molar ratio (1:1) of L-alanine and DL-mandelic acid purchased from LOBA was dissolved in deionised water. The chemical reaction scheme of LADLMAH is shown in Fig. 1. The calculated amount of L-alanine and DL-mandelic acid were thoroughly dissolved in solvent of deionised water. After continuous stirring for homogenous mixture, the synthesized solution was allowed for slow solvent evaporation. As a result of spontaneous nucleation after 2 weeks, the resulting LADLMAH salt was collected. The recrystallization process was used to purify the synthesized salt. The purified salt was dissolved in water solvent and it was magnetically stirred for 6 h. Then LADLMAH solution was filtered, and transferred to crystal growth vessels for slow evaporation to take place at room temperature. Optically colourless and good transparent crystal was obtained by slow evaporation at room temperature (32 °C). The photograph of harvested transparent crystal is shown in Fig. 2.

### 2.2 Solubility of LADLMAH

The solubility is one of the essential criteria to grow bulk and transparent single crystals. The solubility of the LADLMAH was determined using deionised water solvent at different temperatures ranging from 30 to 50 °C at an interval of 5 °C. The required amount of LADLMAH is taken to get the saturated solutions separately with the two solvents

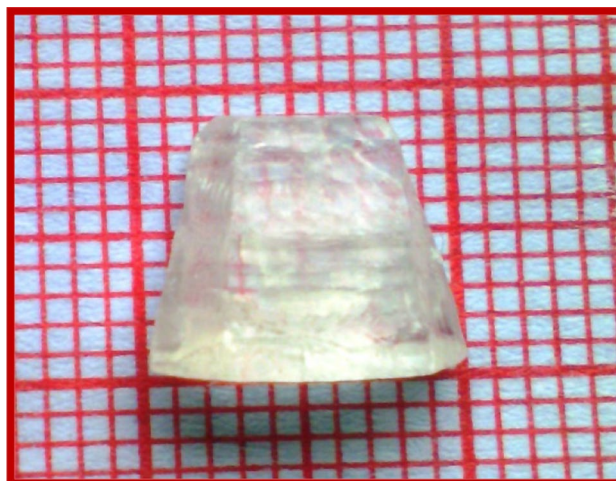


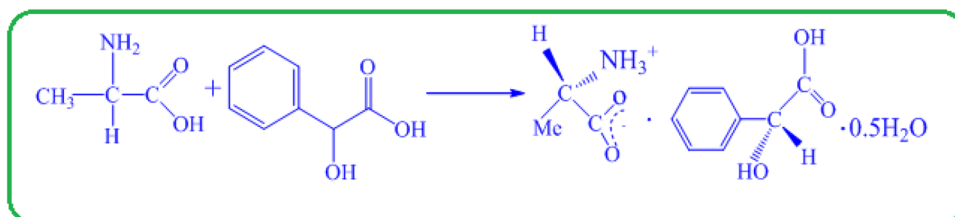
Fig. 2 The grown LADLMAH crystal

(water and ethanol) at various temperatures (30, 35, 40, 45 and 50 °C) and analysed gravimetrically. The solubility of LADLMAH studied for two solvents is illustrated in Fig. 3, which indicates that the solubility increases linearly with the temperature.

### 2.3 Characterization

The grown LADLMAH was exposed to Mo K $\alpha$  ( $\lambda = 0.71073 \text{ \AA}$ ) radiation to measure the cell dimensions by employing a BRUKER KAPPA APEX II CCD diffractometer. A PERKIN ELMER Fourier transform infrared spectrometer was utilized to record the infrared spectrum at room temperature in the range 4000–450  $\text{cm}^{-1}$  by KBr pellet technique. Powder Fourier Transform Raman (FT-Raman) spectrum was recorded on a BRUKER: RFS 27 spectrometer in the range 4000–450  $\text{cm}^{-1}$ . The UV–Vis profile of LADLMAH was obtained at room temperature on a PERKIN ELMER LAMADA 35 spectrophotometer in a wide wavelength range 200–700 nm. A BRUKER AMX 400 spectrometer was utilized to study the carbon–hydrogen framework in the molecule in NMR profile with DMSO as solvent. Thermal analysis was performed in a simultaneous TG/DTA instrument (SII NANO TECHNOLOGY-MODEL TG/DTA 6200 thermal analyser). The experimental conditions were: (i) continuous heating from

Fig. 1 Reaction scheme for LADLMAH compound



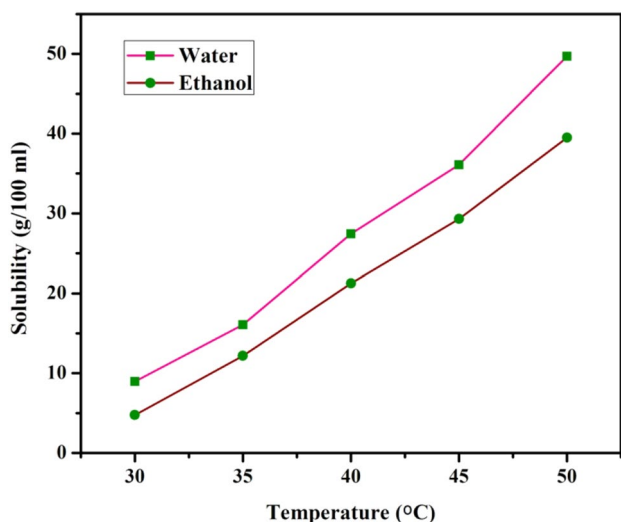


Fig. 3 Solubility curve of LADLMAH compound

room temperature to 500 °C at a heating rate of 20 °C/min, (ii) N<sub>2</sub>—gas dynamic atmosphere (90 cm<sup>3</sup>/min), (iii) alumina, as reference material. To analyse the SHG property, LADLMAH powder was exposed to pulsed Nd:YAG laser (continuum, series) using powder Kurtz Perry method. The LDT value of LADLMAH was also estimated by subjecting one of the hard crystal to Q-switched Nd:YAG laser with fundamental wavelength of 1064 nm and with pulse width 6 ns in the repetition rate of 10 Hz. With effective use of PERKIN ELMER LS 45 spectrofluorophotometer, photoluminescence spectrum was obtained in the range of 300–700 nm. The mechanical property of the grown LADLMAH crystals was analysed by Vickers microhardness measurement. The dielectric loss and dielectric constant as a function of frequency in the selected temperature range (313–373 K) were studied using a HIOKO 3532-50 LCR HiTESTER meter.

### 3 Results and discussion

#### 3.1 Single crystal X-ray diffraction analysis

The grown LADLMAH crystal was subjected to X-ray diffraction analysis to confirm the noncentrosymmetric crystal structure and cell parameters. The LADLMAH crystal crystallized in triclinic crystal system, space group P1 and the cell parameter values are enumerated in Table 1 which is in accordance with literature [7].

Table 1 Single crystal XRD data of LADLMAH

Cell parameters	Present work	Reported work [7]
	Triclinic	Triclinic
Space group	P1	P1
a (Å)	6.02	6.01
b (Å)	8.22	8.22
c (Å)	12.55	12.58
β (°)	88.08	86.00
Volume (Å <sup>3</sup> )	615	616

#### 3.2 FTIR and FT-Raman spectral analyses

Vibrational spectroscopy provides the most definitive means of identifying the various functional groups present in the synthesized compound. In order to analyze the synthesized L-alanine DL-mandelic acid organic chromophore qualitatively, FTIR, FT-Raman spectra were recorded and presented in Figs. 4 and 5 respectively. Free primary amines are characterized by a broad, strong stretching band located in the region 3100–2600 cm<sup>-1</sup> [13]. In accordance with a broad peak located at 3079 cm<sup>-1</sup> for IR, 3073 cm<sup>-1</sup> for FT-Raman both were assigned to NH<sub>3</sub><sup>+</sup> symmetric stretching. The prominent bands positioned at 2572 and 1621 cm<sup>-1</sup> for infrared are specifically due to NH<sub>3</sub><sup>+</sup> asymmetric bending and NH<sub>3</sub><sup>+</sup> asymmetric stretching vibrations. The carboxylate ion group (COO<sup>-</sup>) vibration in infrared spectrum is due to peaks at 1412, 1306, 1154 and 1113 cm<sup>-1</sup> and in FT-Raman spectrum it is due to bands positioned at 1407, 1304, 1175 and 1111 cm<sup>-1</sup> respectively [14]. In all the primary aliphatic compounds containing N–H group showed their stretching vibrations occurring in the region 3500–3300 cm<sup>-1</sup> [15–17].

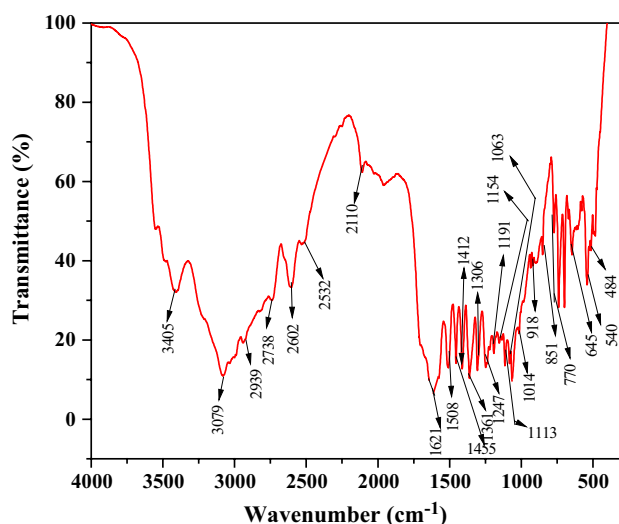


Fig. 4 FTIR profile of LADLMAH

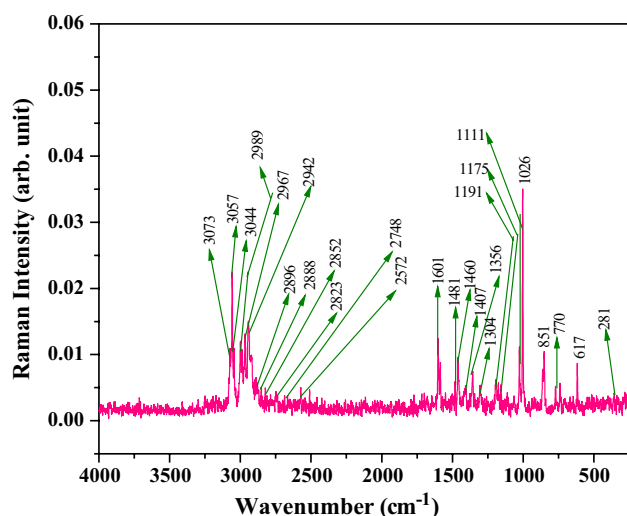


Fig. 5 FT-Raman profile of LADLMAH

The band seen at about 3405 and 1508  $\text{cm}^{-1}$  in FTIR is due to N–H stretching and N–H in plane bending vibrations. The C–C–C asymmetric stretching predicted at 617  $\text{cm}^{-1}$  is an excellent agreement with the experimental observation of FT-Raman spectrum. The characteristic infrared absorption frequencies are normally strong in intensity located in between the region 1400–1200  $\text{cm}^{-1}$  [18]. In the spectrum recorded for the as-grown crystal the peak observed at 1361  $\text{cm}^{-1}$  in IR and 1356  $\text{cm}^{-1}$  in Raman counterpart are attributed to O–H stretching vibrations. The donor and acceptor moieties of carboxylic acid and amino group are held together by the linkage of vander waals type and columbic interactions. Basically C–H stretching mode vibrations appear in the region 3000–2850  $\text{cm}^{-1}$  respectively [18]. Hence in the present investigation, the bands observed at 3057 and 3044  $\text{cm}^{-1}$  in the FT-Raman spectrum are attributed to C–H asymmetric stretching vibrations [18]. The peak positioned at 2939, 2602  $\text{cm}^{-1}$  in IR and 2942, 2896, 2888 and 2852  $\text{cm}^{-1}$  in FT-Raman are assigned to C–H stretching vibrations respectively. In the present investigation C–C–N symmetric stretching vibration occur at wavenumbers 918, 851  $\text{cm}^{-1}$  in infra red and 851  $\text{cm}^{-1}$  in FT-Raman counterpart [14]. The various vibrations and their assignment are enumerated in Table 2.

### 3.3 NMR spectral analysis

The  $^1\text{H}$  NMR and  $^{13}\text{C}$  NMR spectral analysis could be suitably employed in identifying and confirming the structure of organic compounds.  $^1\text{H}$  NMR spectrum of LADLMAH is depicted in Fig. 6. In  $^1\text{H}$  NMR spectrum, triplet peak observed due to the resonance peak in the range 7.2–7.4 ppm confirm the presence of phenolic protons in DL-mandelic acid and also the presence of different proton

Table 2 FTIR, FT-Raman spectral assignments of LADLMAH

Wavenumber ( $\text{cm}^{-1}$ )		Assignments
FT-IR	FT-Raman	
3405		N–H stretching
3079	3073	$\text{NH}_3^+$ symmetric stretching
	3057, 3044	C–H asymmetric stretching
	2989, 2967	$\text{CH}_2$ stretching
2939	2942, 2896	C–H stretching
	2888, 2852	C–H stretching
	2823	Asymmetric $\text{NH}_3^+$ bending + torsion $\text{NH}_3^+$
2738	2748	Asymmetric $\text{NH}_3^+$ bending + torsion $\text{NH}_3^+$
2602		C–H stretching
2532	2572	Asymmetric $\text{NH}_3^+$ bending + torsion $\text{NH}_3^+$
2110		Combination of $\text{NH}_3^+$ asymmetric stretching
1621	1601	$\text{NH}_3^+$ asymmetric stretching
1508		N–H in plane bending
	1482	$\text{CH}_2$ scissoring
1455	1460	C– $\text{NH}_3$ stretching
1412	1407	$\text{COO}^-$ symmetric stretching
1361	1356	O–H deformation
1306	1304	$\text{COO}^-$ asymmetric stretching
1247		C–O asymmetric stretching
1191	1191	$\text{NH}_3^+$ rocking
1154, 1113	1175, 1111	$\text{COO}^-$ asymmetric stretching
1063		C–N asymmetric stretching
1014	1026	C– $\text{NH}_2$ stretching
918, 851	851	C–C–N symmetric stretching
770	770	O–C–O deformation
645		$\text{COO}^-$ scissoring
	617	C–C–C asymmetric stretching
540		$\text{COO}^-$ rocking
	281	$\text{CH}_3$ stretching
484		$\text{NH}_3^+$ torsion

environment in L-alanine in the organic second harmonic generation (SHG) compound LADLMAH. The chemical shift observed at  $\delta = 7.2$  ppm arised due to protonated amino group ( $\text{NH}_3^+$ ) in L-alanine. A singlet developed at  $\delta = 5.0$  ppm is due to carbonyl proton of L-alanine and DL-mandelic acid. The resonance peak at  $\delta = 4.0$  ppm confirms the proton of water molecule in the crystalline compound. The chemical shift observed at  $\delta = 2.5$  ppm shows a downfield to CH proton of DL-mandelic acid. A less intensity peak appear as singlet deshields at  $\delta = 1.3$  ppm can be attributed to the proton in methyl group environment of L-alanine. The  $^{13}\text{C}$  NMR spectrum of LADLMAH is shown in Fig. 7. The signal at 174.5 ppm is assigned to carbon environment in carboxyl group in DL-mandelic acid and chiral L-alanine present in the crystalline compound.

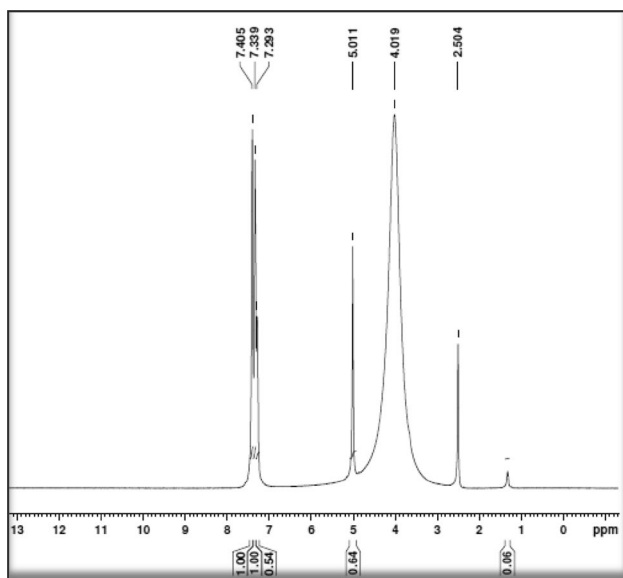


Fig. 6  $^1\text{H}$  NMR profile of LADLMAH

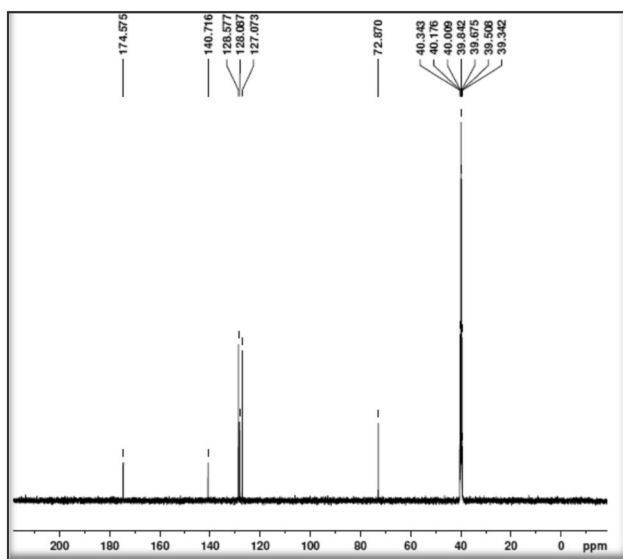


Fig. 7  $^{13}\text{C}$  NMR profile of LADLMAH

Also the resonance peak at 140.7 ppm is safely assigned to carbon atom in the CH environment of DL-mandelic acid present in the crystalline structure. The peaks of different intensities present in the range 127.0–128.5 ppm are attributed to para and meta position of carbon atoms of DL-mandelic acid. The presence of signals between 39.3 and 40.3 ppm is assigned to different carbon environment in L-alanine present in title compound. Thus the NMR analysis of LADLMAH gives clear indication about the structure.

### 3.4 Optical absorption studies

The linear optical properties of LADLMAH crystal was employed to analyze UV–Vis optical absorption study. The optical absorption spectrum recorded in the region 200–700 nm is presented in Fig. 8a. UV–Vis spectrum provides the information about the structure of the molecule because the absorption of UV–Vis light involves shifting of electron from ground state to higher energy states [19]. Since the as-grown crystal is colourless, small absorption is observed in the entire visible region and exhibits maximum transmittance in UV region. Hence it is a desirable property of the crystals in device fabrication [20]. The fundamental lower cut off wavelength is observed at 258 nm. The measured absorbance ( $A$ ) was used to deduce the absorption coefficient ( $\alpha$ ) using the formula,

$$\alpha = \frac{2.3026 \log(1/T)}{t} \quad (1)$$

$t$  is the thickness of the sample, the optical electronic band gap ( $E_g$ ) was computed from the absorption coefficient ( $\alpha$ ) near the absorption edge given by [21]:

$$h\nu\alpha = A(h\nu - E_g)^{1/2} \quad (2)$$

where  $E_g$  is electronic band gap energy,  $h$  is Plank's constant,  $\nu$  is frequency of the incident photons and  $A$  is constant. The band gap energy was evaluated from linear part of the  $\text{tauc}'\text{s}$  plot by plotting  $(h\nu\alpha)^2$  versus  $h\nu$  shown in Fig. 8b. Optical direct band gap value is found to be  $E_g = 5.20$  eV. Hence a grown crystal having such a wide optical band gap suggests its suitability in the field optoelectronic applications.

### 3.5 NLO studies

Nonlinear optics (NLO) is the study of phenomena that result from a field induced modification in the optical properties of a material system [22]. The SHG conversion efficiency of LADLMAH was investigated by Kurtz and Perry powder technique, [21] and the efficiency of LADLMAH sample was compared with the microcrystalline powder of KDP. LADLMAH was analyzed using spectra physics quanta Nd:YAG laser with first harmonics output (1064 nm, 10 ns, 10 Hz) with 0.689 J pulse energy as the radiation source. The output emission of green radiation from the LADLMAH crystal confirms the SHG in the crystal. The calculated SHG efficiency of LADLMAH is about 0.65 times that of KDP. Some of the reported organic chromophores with space group and NLO efficiency are listed in Table 3 for comparison along with SHG experiment observation of as-grown crystal.

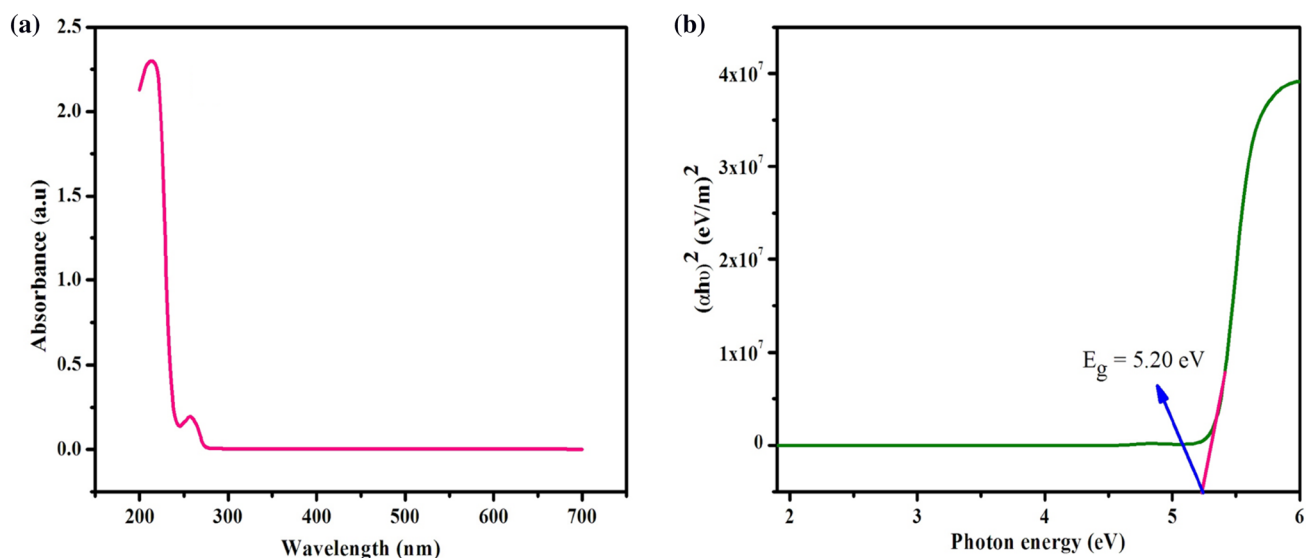


**Fig. 8** **a** UV–Vis profile and **b** Tauc's plot of LADLMAH

**Table 3** A comparison NLO efficiency of non-centrosymmetric crystals

Crystal	Space group	NLO efficiency	References
L-Phenylalanine nitric acid	P2 <sub>1</sub>	0.26	[23]
L-Alanine	P2	0.33	[24]
L-Phenylalanine DL-mandelic acid	C2	0.35	[25]
L-Phenylalanine benzoic acid	P2 <sub>1</sub>	0.56	[26]
L-Alanine DL-mandelic acid	P1	0.65	Present work

### 3.6 Thermal studies

Thermogram gives information about decomposition nature of material where the weight loss occurs at different stages [27]. Thermogravimetric analysis (TGA) and differential thermal analysis (DTA) were carried out for LADLMAH using SII NANO TECHNOLOGY (MODEL TG/DTA 6200) between the temperature 50 and 500 °C at a heating rate of 20 °C/min under nitrogen atmosphere. The TG/DTA spectrum of LADLMAH is shown in Fig. 9. In the observed DTA curve a minute endothermic peak at 99.4 °C is due to adsorption of entrapped water in the grown crystal, showing a low temperature of the decomposition. The first and second stage of weight loss occur in the temperatures 133.9 and 240 °C showing a weight loss, due to the decomposition and volatilization of the title compound. The final stage of decomposition is observed between 240 and 360 °C, where complete decomposition of the residue is observed. The DTA trace clearly shows that the compound thermally stable up to 133.9 °C. Hence we can conclude that the LADLMAH is suitable for NLO application up to 133.9 °C.

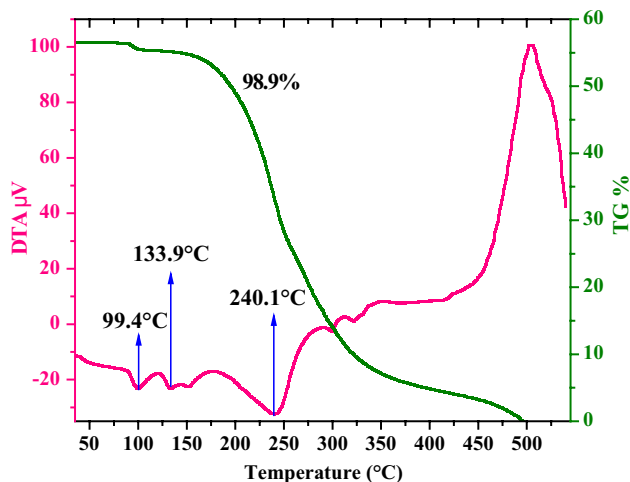


**Fig. 9** TG–DTA profile of LADLMAH

### 3.7 Surface laser damage threshold (LDT) measurement

One of the supportive criteria for a NLO crystal depends not only on the linear and nonlinear properties but also greatly

on its ability to withstand high power lasers [28]. Laser-induced damage threshold studies on nonlinear optical crystals are essential as the surface damage of the crystal by high power lasers employed enhance their performance in nonlinear optical applications [29]. Therefore, the performance of the crystal strongly depends on quality of surface. The multiple shot laser damage threshold value of LADLMAH crystal has been measured by using Q-switched Nd:YAG laser (1064 nm with pulse width of 6 ns and the repetition rate of 10 Hz). The surface damage threshold value of the LADLMAH crystal were calculated using the power density expression,

$$\text{Power density } (P_d) = E/\tau\pi r^2 \text{ (GW/cm}^2\text{)} \quad (3)$$

where E is energy (mJ),  $\tau$  is the pulse width (ns) and r is the radius of the spot (mm). The calculated surface damage energy density of crystal for multiple shot is found to be 5.074 GW/cm<sup>2</sup>. The laser damage profile of the LADLMAH crystal is presented in Fig. 10. The higher value of laser-induced damage threshold will be useful for making laser based devices. The result of LDT was compared with the other organic crystals listed in Table 4.

### 3.8 Microhardness studies

Hardness of the material carries information about the strength, molecular bindings, yield strength and elastic stiffness constant [21]. The mechanical strength of the materials plays a significant key role in device fabrication. The hardness measurement on a crystal provides information about the elastic, plastic, viscous and fracture properties. The Vickers microhardness measurement convicts the mechanical property of grown LADLMAH crystal. The mechanical hardness test was carried out at room temperature and loads of alternate magnitudes such as 25, 50 and 100 g were applied. For

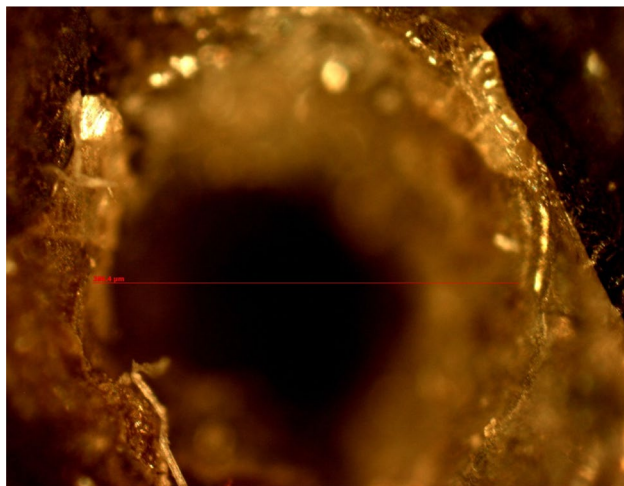


Fig. 10 Laser damage profile of LADLMAH

Table 4 Comparison of laser damage threshold values

Crystal	Laser damage threshold value (GW/cm <sup>2</sup> )	References
Potassium dihydrogen phosphate (KDP)	0.2	[22]
Urea	1.5	[22]
Dimethyl amino pyridinium 4-nitrophenolate 4-nitrophenol	2.24	[22]
Guanidinium phenyl arsonate	4.07	[22]
L-Phenylalanine DL-mandelic acid	4.98	[22]
L-Alanine DL-mandelic acid	5.07	Present work

a specified load at least five well-defined impressions were referred and the average of the all the diagonals (d) were considered. The Vickers microhardness number is calculated using the expression,

$$H_v = 1.855 (P/d^2) \quad (4)$$

where  $H_v$ , P, d are Vickers hardness number in kg/mm<sup>2</sup>, the indenter load in kg, the diagonal length of the indented impression in mm. Figure 11a evince the variation of hardness number ( $H_v$ ) as an event of applied load ranging from 25 to 100 g for LADLMAH crystal. It is noted from the figure that hardness ( $H_v$ ) increases with increasing applied indentation load, which can be considered as the reverse indentation size effect (RISE) [21]. The size of indentation and load are relevant through Meyer's law [22],

$$P = K_1 d^n \quad (5)$$

(or)

$$\log P = \log K_1 + n \log d \quad (6)$$

where  $K_1$  is the standard hardness constant and 'n' the Meyer's index also known as work hardening coefficient. The value of work hardening coefficient (Meyers index number) 'n' is evaluated from the graph plotted between log P versus log d and is shown in Fig. 11b. The slope of the straight line of graph gives the value of 'n' evaluated as 2.73. For the regular ISE behaviour we have  $n < 2$ . When  $n > 2$ , there is a reverse ISE behaviour. This is in good consent with the experimental data and thus confirms the reverse ISE behaviour. As per Onitsch [30], Meyers index 'n' should lies between 1 and 1.6 for hard materials and above 1.6 for soft materials. Hence LADLMAH can be labelled under the category of soft materials.

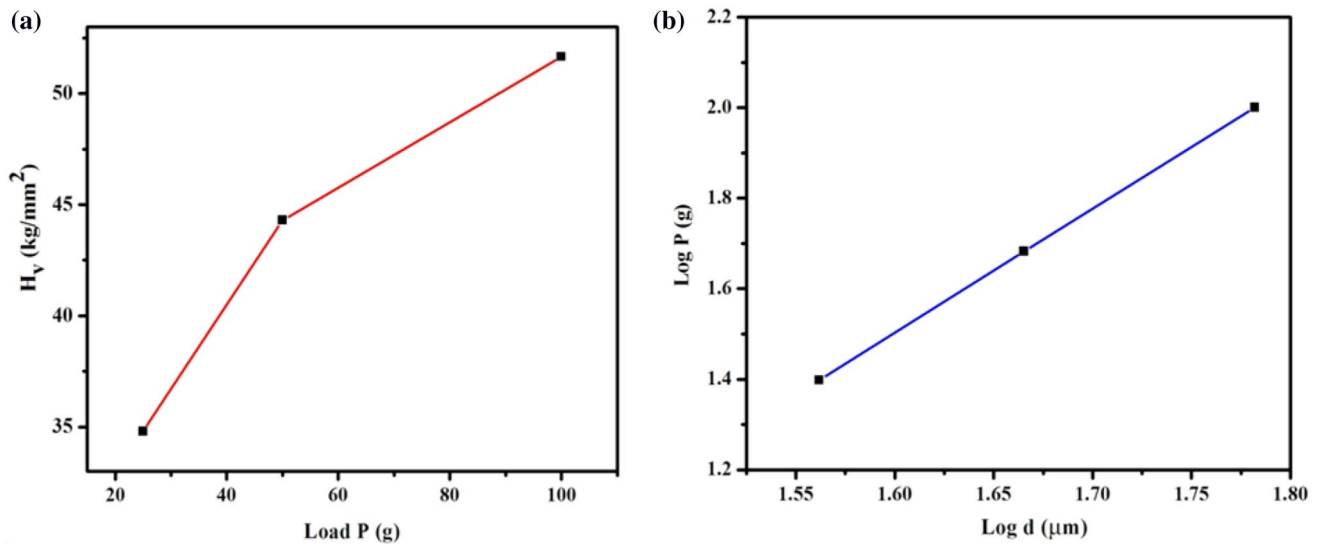


Fig. 11 a Hardness value and b Mayer's plot of LADLMAH

### 3.9 Dielectric studies

The dielectric property is one of the indispensable properties to know the electrical response of the solids. Dielectric properties deal with the electro-optic property of the crystals. The analysis of dielectric properties gives knowledge about electric fields within the solid materials. The dielectric study of LADLMAH was carried out for various temperatures 313, 333, 353, and 373 K in the frequency range 50 Hz–5 MHz respectively. The real part of the dielectric constant ( $\epsilon'$ ) of the crystal has been calculated using the relation,

$$\epsilon' = \frac{Cd}{A\epsilon_0} \quad (7)$$

where  $C$  is the capacitance,  $d$  is the thickness of the crystal,  $\epsilon_0$  is the vacuum dielectric constant and  $A$  is the area of the crystal. The imaginary part of the dielectric constant ( $\epsilon''$ ) of the crystal was assessed calculated using the relation,

$$\epsilon'' = \epsilon' \tan \delta \quad (8)$$

where  $\tan \delta$  is the loss tangent. Figure 12a, b shows that the variation of dielectric constant ( $\epsilon'$ ) and dielectric loss ( $\epsilon''$ ) versus logarithm of frequency at various temperatures. Variation of dielectric constant, dielectric loss with temperature is mainly ascribed to the crystal expansion, the electronic, space charge, orientational and ionic polarizations and the presence of dopants and crystal defects. From the graphs,

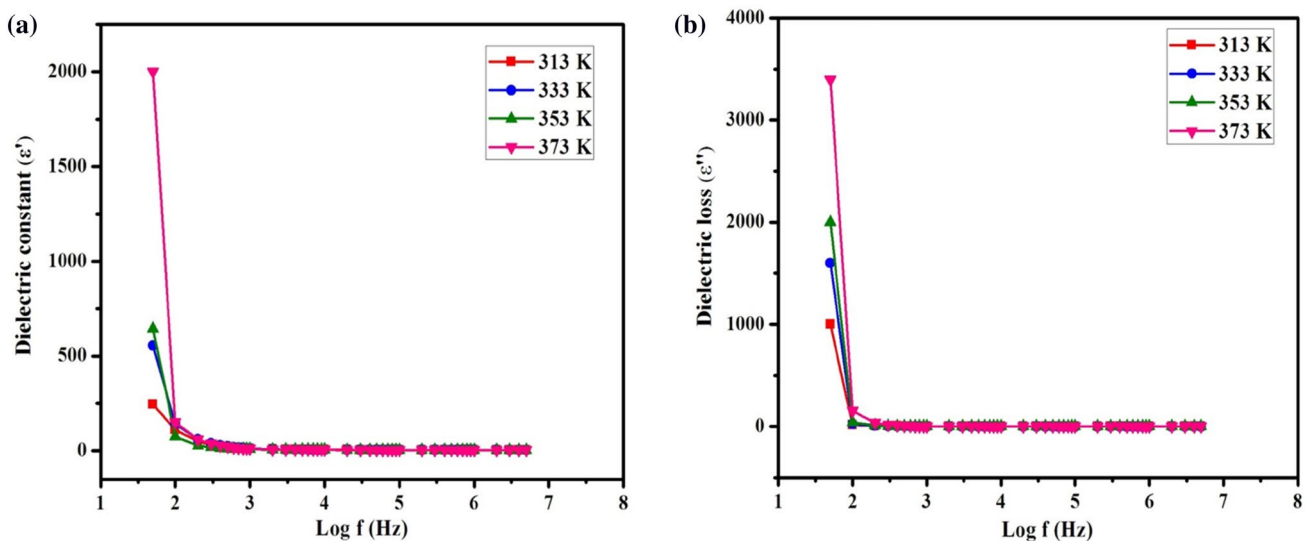


Fig. 12 Plot of a  $\log f$  versus dielectric constant and b  $\log f$  versus dielectric loss



it clearly depict that the values of dielectric constant and dielectric loss decreases with the increase in frequency. The very high value of dielectric constant ( $\epsilon'$ ) at low frequencies may be due to the occurrence of above four polarizations as stated. The low value of dielectric constant ( $\epsilon'$ ) at high frequencies may be due to the loss of consequence of these polarizations gradually [26]. The low dielectric loss and dielectric constant at higher frequencies reveals the lesser defects with high optical quality of the LADLMAH crystal, which is also meet the requirements in opto-electronic applications and NLO devices [26].

### 3.10 Z-scan measurements

Third-order nonlinear optical susceptibility ( $\chi^{(3)}$ ), nonlinear refractive (NLR) index ( $n_2$ ) and nonlinear absorption (NLA) coefficient ( $\beta$ ) for the grown material were calculated from the measurements of Z-scan using continuous wave Nd:YAG laser of wavelength 532 nm with power 42 mW. Closed aperture and open aperture Z-scan results in LADLMAH crystals

were subjected to measuring NLA coefficient and NLR index, respectively. Figure 13a, b shows the closed and open aperture of the normalized transmittance plotted as a function of sample position Z. From the closed aperture Z-scan curve we observed that the peak followed by a valley-normalized transmittance, which is suggest that the third-order NLR index change in negative, i.e., the occurrence of self-defocusing. The open aperture curve Fig. 13b reveals that the transmittance of crystal gains minimum value at the focus ( $Z=0$ ). The mode of open aperture curve confirmed the occurrence of saturable absorption (SA) in LADLMAH crystal. The ratio of the closed-to-open normalized Z-scan curve presented in Fig. 13c. The on-axis phase shift  $\Delta\Phi$  at the focus is related to third-order NLR index of the crystal by,

$$n_2 = \frac{\Delta\Phi_0}{KI_0L_{eff}} \tag{9}$$

where K is the wave vector ( $K = 2\pi/\lambda$ ),  $\lambda$  is the laser wavelength,  $I_0$  is the intensity of the laser beam at the focus

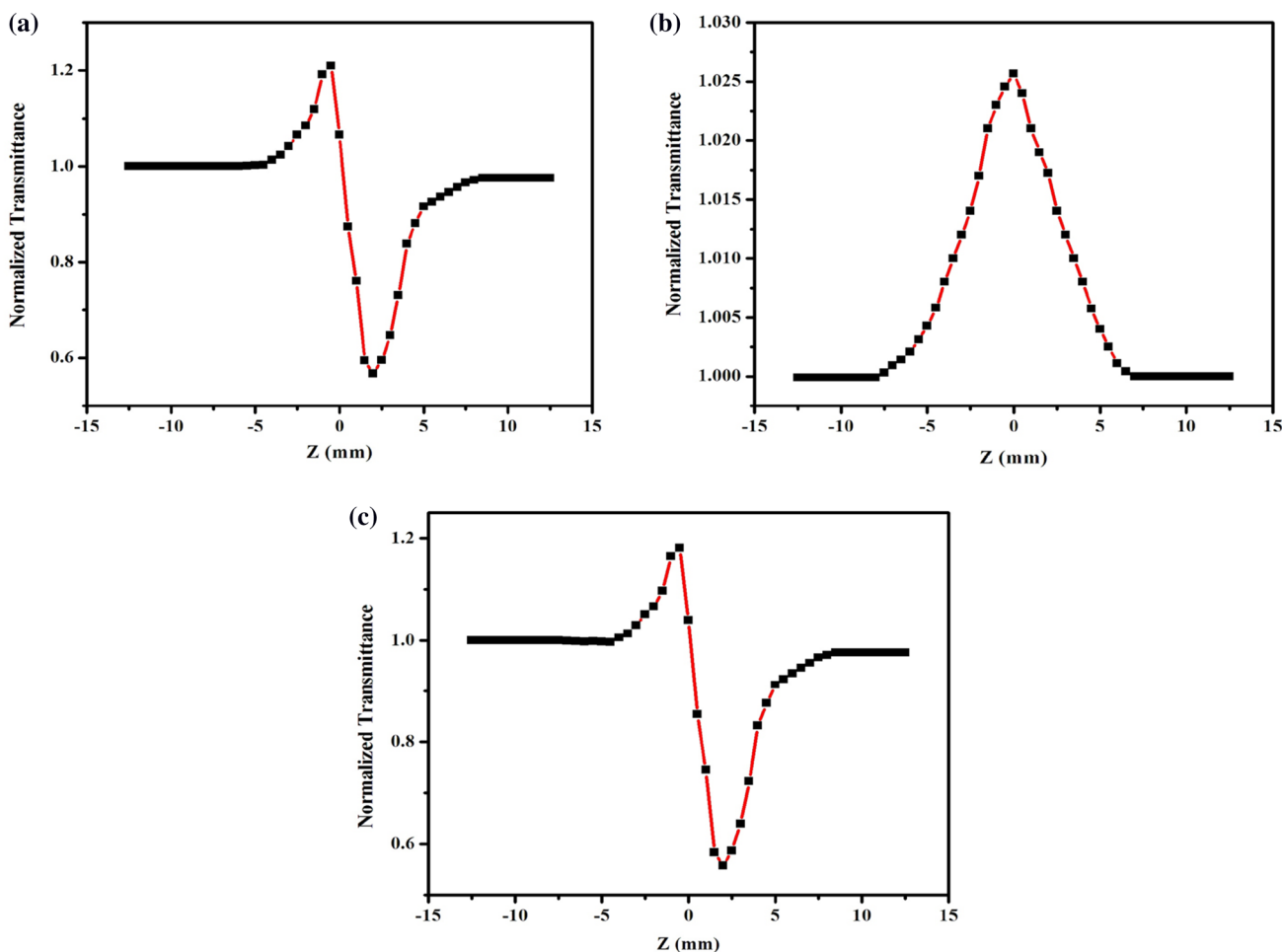


Fig. 13 a Closed aperture, b open aperture and c ratio of the closed-to-open Z-scan traces of LADLMAH

( $Z=0$ ).  $L_{eff} = [1 - \exp(-\alpha L)]/\alpha$  is the effective thickness of the sample,  $\alpha$  and  $L$  is the linear absorption coefficient and the thickness of the crystal respectively. From the open aperture trace, the NLA coefficient ( $\beta$ ) is estimated using the relation,

$$\beta = \frac{2\sqrt{2}\Delta T}{I_0 L_{eff}} \quad (10)$$

where  $\Delta T$  is the one valley value at the open aperture Z-scan trace. The value of  $\beta$  takes the negative value for saturated absorption and positive for two-photon absorption processes. The real and imaginary parts of the third-order nonlinear optical susceptibility  $\chi^{(3)}$  were evaluated from experimental determination of  $n_2$  and  $\beta$  in regard to the following relations,

$$\text{Re } \chi^{(3)}(\text{esu}) = \frac{10^{-4}(\epsilon_0 C^2 n_o^2 n_2)}{\pi} \left( \frac{\text{cm}^2}{\text{W}} \right) \quad (11)$$

$$\text{Im } \chi^{(3)}(\text{esu}) = \frac{10^{-2}(\epsilon_0 C^2 n_o \lambda \beta)}{4\pi^2} \left( \frac{\text{cm}^2}{\text{W}} \right) \quad (12)$$

where  $\epsilon_0$  is the permittivity of free space ( $8.8518 \times 10^{-12}$  F/m),  $n_0$  is the linear refractive index of the crystal and  $C$  is the velocity of the light in a vacuum. The absolute value of third-order nonlinear optical susceptibility  $\chi^{(3)}$  was calculated from the following relation,

$$|\chi^{(3)}| = \sqrt{(\text{Re}(\chi^{(3)}))^2 + (\text{Im}(\chi^{(3)}))^2} \quad (13)$$

The coupling factor  $\rho = [\text{Im}(\chi^{(3)})/\text{Re}(\chi^{(3)})]$  is the ratio of the imaginary part ( $\text{Im}(\chi^{(3)})$ ) to the real part ( $\text{Re}(\chi^{(3)})$ ) of third-order nonlinear optical susceptibility. The estimated coupling factor  $\rho$  was found to be (0.0268). Table 5 portrays the experimental details and the results of the Z-scan technique for LADLMAH crystal. The third-order susceptibility is found to be comparably larger than the other well-known

NLO crystals in Table 6. The NLA is ascribed to saturation absorption process and nonlinear refraction (NLR) leads to the self-defocusing nature in the crystal. Thus, the LADLMAH can be a versatile material for NLO device fabrications.

## 4 Conclusion

An efficient SHG crystal LADLMAH was synthesized and grown from deionized water by slow solvent evaporation technique. The single crystal X-ray diffraction study confirmed that the LADLMAH grown crystal belongs to the triclinic system with non-centrosymmetric space group P1. The vibrational and nuclear magnetic resonance (NMR) analysis identifies the functional groups that contribute the grown crystal. From UV–Vis profile, optical band gap were found to be 5.20 eV. The nonlinear optical test reveals that LADLMAH exhibit powder SHG efficiency of 0.65 times that of  $\text{KH}_2\text{PO}_4$  (KDP). The thermal analysis study by TG/DTA techniques reveals the thermal stability of the title compound. It is noticed that the surface laser-induced damage (LDT) threshold value ( $5.07 \text{ GW/cm}^2$ ) is higher than that of  $\text{KH}_2\text{PO}_4$  (KDP) and urea. From the microhardness study, we conclude that the LADLMAH crystal belongs to a soft material category. The dielectric study proves that the LADLMAH exhibit low dielectric constant and dielectric loss at high frequency region. Z-scan technique revealed that the LADLMAH crystal has self-defocusing nature with a positive NLA coefficient. By these concerns, the

**Table 6** Comparison of  $\chi^{(3)}$  values of LADLMAH with other NLO materials

Crystal	Third-order susceptibility $\chi^{(3)}$	References
LADLMAH	$5.84 \times 10^{-6}$ esu	Present work
LAPA	$5.24 \times 10^{-7}$ esu	[31]
GUCN	$2.05 \times 10^{-8}$ esu	[32]
VMST	$9.69 \times 10^{-12}$ esu	[33]

**Table 5** Obtained nonlinear optical parameters from Z-scan measurements for LADLMAH

Parameters	Measured values for LADLMAH crystal
Laser beam wavelength ( $\lambda$ )	532 nm
Linear absorption coefficient ( $\alpha$ )	0.899
Nonlinear refractive index ( $n_2$ )	$4.355 \times 10^{-8} \text{ cm}^2/\text{W}$
Nonlinear absorption coefficient ( $\beta$ )	$0.025 \times 10^{-4} \text{ cm/W}$
Real part of the third-order susceptibility [ $\text{Re}(\chi^3)$ ]	$5.845 \times 10^{-6}$ esu
Imaginary part of the third-order susceptibility [ $\text{Im}(\chi^3)$ ]	$0.157 \times 10^{-6}$ esu
Third-order nonlinear optical susceptibility ( $\chi^3$ )	$5.847 \times 10^{-6}$ esu

LADLMAH crystal could be a promising and a competitive candidate for future opto-electronic applications.

**Acknowledgements** The scientific supports extended by sophisticated analytical instruments facility (SAIF), Indian Institute of Technology (IITM) for support in single crystal XRD, FTIR, FT-Raman and NMR measurement.

## References

1. M.D. Aggarwal, J. Choi, W.S. Wang, K. Bhat, R.B. Lal, A.D. Shields, B.C. Penn, D.V. Frazier, J. Cryst. Growth **204**, 179 (1999)
2. P.N. Prasad, D.J. Williams, *Introduction to Nonlinear Optical Effect in Molecules and Polymers* (Wiley, New York, 1991)
3. J.L. Oudar, J. Zyss, Phys. Rev. A **26**, 2016 (1982)
4. R. Hanumantharao, S. Kalainathan, Spectrochim. Acta A **86**, 80 (2012)
5. A.S.J. Lucia Rose, P. Selvarajan, S. Perumal, Spectrochim. Acta A **81**, 270 (2011)
6. A.S.J. Lucia Rose, P. Selvarajan, S. Perumal, Physica B **406**, 412 (2011)
7. Z.-Q. Hu, D.-J. Xu, Y.-Z. Xu, J.-Y. Wu, M.Y. Chiang, Acta Crystallogr. C **58**, 0612 (2002)
8. M. Babji, A. Mondry, J. Rare Earths **29**, 1188 (2011)
9. H.-S. Guo, J.-M. Kim, S.-M. Chang, W.-S. Kim, Biosens. Bioelectron. **24**, 2931 (2009)
10. P. Michal Babij, A. Starynowicz, Mondry, J. Mol. Struct. **1006**, 672 (2011)
11. M. Badawi, W. Forner, Spectrochim. Acta A **78**, 1162 (2011)
12. D.J.C. Gomes, F.J. Caires, L.S. Lima, A.C. Gigante, M. Ionashiro, Thermochem. Acta **533**, 16 (2012)
13. R.M. Silverstein, F.X. Webster, *Spectrometric Identification of Organic Compounds* (Wiley, New York, 2005)
14. P. Ilayabarathi, J. Chandrasekaran, Spectrochim. Acta A **96**, 684 (2012)
15. S. Mohan, N. Puviarasan, S. Bakkialakshmi, Asian J. Chem. **11**, 1337 (1999)
16. A. Altun, K. Golcuk, M. Kumru, J. Mol. Struct. **637**, 155 (2003)
17. N. Puviarasan, V. Arjuna, S. Mohan, J. Chem. **26**, 323 (2002)
18. G. Socrates, *Infrared and Raman Characteristic Group Frequencies*, 3rd edn. (Wiley, Chichester, 2001)
19. P. Krishnan, K. Gayathri, G. Bhagavannarayana, S. Gunasekaran, G. Anbalagan, Spectrochim. Acta A **102**, 379 (2013)
20. P. Jayaprakash, M. Peer Mohamed, M. Lydia Caroline, J. Mol. Struct. **1134**, 67 (2017)
21. R. Robert, C. Justin Raj, S. Krishnan, S. Jerome Das, Physica B **405**, 20 (2010)
22. P. Jayaprakash, M. Peer Mohamed, P. Krishnan, M. Nageshwari, G. Mani, M. Lydia Caroline, Physica B **503**, 25 (2016)
23. J.A. Miragliotta, Appl. Res. **16**, 4 (1995)
24. M. Lydia Caroline, R. Sankar, R.M. Indirani, S. Vasudevan, Mater. Chem. Phys. **114**, 490 (2009)
25. M. Lydia Caroline, S. Vasudevan, Mater. Lett. **63**, 41 (2009)
26. P. Jayaprakash, P. Sangeetha, C. Rathika Thaya Kumari, I. Baskaran, M. Lydia Caroline, J. Mater. Sci.: Mater. Electron. **28**, 18787–18794 (2017)
27. F. Meng, M.K. Lu Yang, H. Zeng, Mater. Lett. **33**, 265 (1998)
28. E.D. D'silva, D. Narayan Rao, R. Philip, R.J. Butcher, Rajnikant, S.M. Dharmaparakash, J. Phys. Chem. Solids **72**, 824 (2011)
29. P. Krishnan, K. Gayathri, N. Sivakumar, S. Gunasekaran, G. Anbalagan, J. Cryst. Growth **396**, 85 (2014)
30. E.M. Onitsch, Mikroskopie **2**, 131 (1947)
31. R. Jothi Mani, P. Selvarajan, H. Alex Devadoss, D. Shanthi, Optik **126**, 213 (2014)
32. M. Dhavamurthy, R. Raja, K. Syed Suresh Babu, R. Mohan, Appl. Phys. A (2016). <https://doi.org/10.1007/s00339-016-0219-0>
33. M.K. Kumar, S. Sudhakar, P. Pandi, G. Bhagavannarayana, R.M. Kumar, Opt. Mater. **36**, 988 (2014)